Journal of Computational Physics 230 (2011) 13–26

Contents lists available at ScienceDirect

Journal of Computational Physics

journal homepage: www.elsevier.com/locate/jcp

Adaptive mesh refinement for stochastic reaction–diffusion processes

Basil Bayati, Philippe Chatelain, Petros Koumoutsakos *

Chair of Computational Science, ETH Zurich, CH-8092, Switzerland

ARTICLE INFO

Article history:
Received 4 February 2010
Received in revised form 5 July 2010
Accepted 30 August 2010
Available online 16 September 2010

Keywords:
AMR
Stochastic simulations
Reaction–diffusion

ABSTRACT

We present an algorithm for adaptive mesh refinement applied to mesoscopic stochastic simulations of spatially evolving reaction–diffusion processes. The transition rates for the diffusion process are derived on adaptive, locally refined structured meshes. Convergence of the diffusion process is presented and the fluctuations of the stochastic process are verified. Furthermore, a refinement criterion is proposed for the evolution of the adaptive mesh. The method is validated in simulations of reaction–diffusion processes as described by the Fisher–Kolmogorov and Gray–Scott equations.

1. Introduction

Simulations of systems that exhibit multiple spatial scales often employ adaptive mesh refinement methods (AMR) [1,2] for the discretization of the governing partial differential equations (PDEs). However, when the mesh spacing approaches the molecular scale and thermal fluctuations affect the dynamics of the system, the use of partial differential equations may become unjustifiable for variables that are inherently random and discrete [3–5]. At the same time simulations of microscopic phenomena may not be efficiently computed using atomistic level modeling as in molecular dynamics (MD). There is an increased interest [6–14] in formulating methods for mesoscopic simulations in which the computational elements contain neither so many particles as to be considered in a continuum, nor so few as to warrant MD simulations. Such mesoscopic simulations employ variables that are assumed to be governed by the laws of probability theory. The transition probabilities of any discrete-state, continuous-time Markov process must obey the *Chapman–Kolmogorov* equation, which in turn is equivalent to the so-called *master equation* (M-equation) [15]. Since the number of states is large – possibly infinite – for all but the simplest systems, analytical or direct numerical integration methods for the M-equation are generally impractical. Being at a loss for a direct solution, numerical realizations of the stochastic process can alternatively be generated. These numerical realizations, performed via *stochastic simulation algorithms* [16,17], amount to generating random variates from the unknown discrete probability density function.

The M-equation frequently appears in chemical kinetics since the time-evolution of chemically-reacting species in a system is inherently stochastic owing to Brownian motion [18,19]. The applicability of the M-equation to chemical kinetics rests on the assumption that the system is in thermal equilibrium, such that any molecule has enough time, on average, to move throughout the volume before it participates in a reaction. If Brownian motion does not suffice, then the system is inhomogeneous and the problem has intrinsically local phenomena. The variables in the system are recast to represent the number of molecules of a species in a subvolume – or volume element – of space. This description has been previously studied theoretically [6–8] and numerically [9] using a uniform discretization in 1-D. Moreover, 2- and 3-D uniform discretizations have been used for simulating nonlinear reaction–diffusion processes [12]. Since inhomogeneities may arise at various scales

* Corresponding author. Tel.: +41 1 632 5258; fax: +41 1 632 1703.
E-mail addresses: petros@ethz.ch, petros@inf.ethz.ch (P. Koumoutsakos).

0021-9991/$ - see front matter © 2010 Elsevier Inc. All rights reserved.
doi:10.1016/j.jcp.2010.08.035

throughout the domain, the placement of smaller or larger volume elements in certain regions of the domain readily lends itself to finite volume methods [20]. Non-uniform 1-D discretizations, which have borrowed techniques from finite volume methods, have been employed for propagating wavefront systems [10,11]. Recently, Engblom et al. [13] and Ferm et al. [21] have used adaptive and unstructured meshes in simulations of stochastic processes. Additionally, Drawert et al. [22] have used the Finite State Projection algorithm presented in [23] to simulate reaction–diffusion processes.

This work is concerned with formulating the transition rates, or *propensities*, for reaction–diffusion processes on adaptive locally refined structured meshes in the spirit of *adaptive mesh refinement* (AMR) [1,2,24], and simulating mesoscopic reaction–diffusion processes using these rates. The convergence of the diffusion process is presented as well as a refinement criterion for the adaptive mesh. The method is applied to relatively high spatial-resolution simulations of the *Fisher–Kolmogorov* [25] and *Gray–Scott* [26] equations. The results indicate that the method is especially suited for, but not limited to, wavefront propagation and pattern formation problems.

The paper is organised as follows: Sections 1.1 and 1.2 introduce the master equation and stochastic simulation algorithms, respectively. Section 2 presents a derivation for diffusion propensities on locally refined meshes, and Section 3 recapitulates reaction propensities and their validity with respect to the spatial discretization. Section 4 presents the mesh refinement criterion and stochastic interpolation method used in this study. Section 5 shows both the validity of the method and numerical examples, and Section 6 concludes this work.

1.1. Master equation

Let $\mathcal{G} \subset \mathbb{R}^d$ denote the domain in which stochastic reaction and diffusion processes reside. Following the notation presented in [27], let $\mathcal{G}$ be subdivided into a collection of voxels, or volume elements, labelled by vectors $\mathbf{i}$ that belong to an index set, namely $\mathbf{i} \in \mathcal{I}$. Given S species in $\mathcal{G}$, let the time-dependent random variable $U_{\mathbf{i}}^{(s)}(t)$ denote the number of molecules (or particles) of species s in volume element $\mathbf{i}$ at time t. Furthermore, define $\mathbf{U}_{\mathbf{i}} \triangleq \left(U_{\mathbf{i}}^{(1)}, \ldots, U_{\mathbf{i}}^{(S)}\right)$, $\mathbf{U}^{(s)} \triangleq \left\{U_{\mathbf{i}}^{(s)}\right\}_{\mathbf{i}\in\mathcal{I}}$, and $\mathbf{U}(t) \triangleq \{\mathbf{U}_{\mathbf{i}}\}_{\mathbf{i}\in\mathcal{I}}$.

The reaction–diffusion master equation (RDME) describes the time evolution of a probability density function:

$$\begin{aligned}\frac{\mathrm{d}p(\mathbf{U},t)}{\mathrm{d}t} &= \sum_{\mathbf{i}\in\mathcal{I}}\sum_{\mathbf{j}\in\mathcal{I}}\sum_{s=1}^{S}\left\{a_{\mathbf{i},\mathbf{j}}^{(s)}\left(\mathbf{U}^{(s)}+1_{\mathbf{i}}^{(s)}\right)p\left(\mathbf{U}+1_{\mathbf{j}}^{(s)}-1_{\mathbf{i}}^{(s)},t\right)-a_{\mathbf{j},\mathbf{i}}^{(s)}\left(\mathbf{U}^{(s)}\right)p(\mathbf{U},t)\right\}\\ &\quad+\sum_{\mathbf{i}\in\mathcal{I}}\sum_{m=1}^{M}\left\{a_{\mathbf{i}}^{(m)}(\mathbf{U}_{\mathbf{i}}-\boldsymbol{\nu}^{(m)})p(\mathbf{U}-\boldsymbol{\nu}^{(m)}1_{\mathbf{i}},t)-a_{\mathbf{i}}^{(m)}(\mathbf{U}_{\mathbf{i}})p(\mathbf{U},t)\right\},\end{aligned} \tag{1}$$

where the diffusion process has been modeled as the movement of a molecule to a neighboring volume element [6,10]; $a_{\mathbf{i},\mathbf{j}}^{(s)}(\cdot)$, the so-called propensity function, represents the probability per unit time of the diffusion of a molecule from volume element $\mathbf{j}$ to $\mathbf{i}$; $a_{\mathbf{i}}^{(m)}(\cdot)$ denotes the propensity of reaction m, where $m = 1,\ldots,M$; $\boldsymbol{\nu}^{(m)}$ represents the stoichiometric vector of reaction m; and $1_{\mathbf{i}}^{(s)}$ denotes one molecule of species s at index $\mathbf{i}$ (i.e. $\mathbf{U}(t) + 1_{\mathbf{i}}^{(s)} = U_{\mathbf{i}}^{(s)}(t) + 1$).

1.2. Stochastic simulation algorithms

Eq. (1) constitutes a set of ordinary differential equations. Note that the evolution of the probability density function is determined by the time-dependent propensity functions $a_{\mathbf{i},\mathbf{j}}^{(s)}(\cdot)$ and $a_{\mathbf{i}}^{(m)}(\cdot)$, which represent the unscaled probabilities per unit time of their representative reactions. Since the diffusion events are modeled as unimolecular transitions to neighboring cells, Eq. (1) can be completely characterized by a set of propensities that vary over time. Indeed, stochastic simulations work by generating random variates from the probability density function $p(\mathbf{U},t)$ at every time-step. Stochastic simulations therefore simulate the underlying Markov process, which is defined by the time-dependent propensities.

Given an initial vector of the state space $\mathbf{U}_{sim}$, stochastic simulation algorithms proceed as follows:

$$\Theta(t) \triangleq (\hat{a}_1(t),\ldots,\hat{a}_W(t)), \tag{2}$$

$$\tau \sim \zeta(\Theta(t),\epsilon), \tag{3}$$

$$k^{(w)} \sim \Psi(\Theta(t),\tau), \tag{4}$$

$$\mathbf{U}_{sim}(t+\tau) = \mathbf{U}_{sim}(t) + \sum_{w=1}^{W} k^{(w)}\boldsymbol{\nu}^{(w)}, \tag{5}$$

where $\Theta(t)$ represents propensities $\hat{a}_w(t)$ only from the current state to all other of the W reachable states, where W is the sum of the diffusion and reaction events; the vector $\boldsymbol{\nu}^{(w)}$ denotes the change induced by transformation w; and the distributions ζ and Ψ vary depending on the algorithm that is used (see [18] for a review). These algorithms proceed by iterating through Eqs. (2)–(5) until the predefined final time t_f is reached. Ultimately, $\mathbf{U}_{ssa}(t_f)$ is an approximate random variate from $p(\mathbf{U},t_f)$. Specifically, the relationship between the approximate and exact solution is:

$$p(\mathbf{U},t_f) - p(\mathbf{U}_{sim}(t_f)) \approx C_1\epsilon + C_2N^{-1/2} + C_3h^2, \tag{6}$$

where $C_1\epsilon$ is the error from the integration over time of the stochastic simulation ($\epsilon = 0$ in the case of exact simulation algorithms [17,28]), $C_2N^{-1/2}$ is the well-known sampling error of Monte Carlo methods, and C_3h^2 is the error from the spatial-discretization of the diffusion process.

2. Diffusion

The objective of this derivation is to determine the rates of transitions that represent diffusion for non-uniform volume elements. Following the work presented in [10], the rates will be derived by virtue of a finite volume method. The well-known transition rate for uniformly sized volume elements, D/h^2, will be derived again for the sake of completeness. It should be noted that the jump rates will be chosen to reproduce the statistics of random walks (see Section 5.1.2 and [10]) and to conform to a discretization of the Laplace operator (see Section 5.1.1 and [27]). Specifically, the differential equations derived in the section – in which differentiation relies upon the continuum limit – will be used to determine (i) the propensities for a discrete-space, continuous-time random walk on a non-uniform lattice and (ii) the rate at which the equations converge to the solution of the diffusion equation. In the limit of a large number of molecules, the scaled propensities ought to converge to the continuum equations [29] and this is satisfied, by construction, in this derivation.

The diffusion process on locally refined meshes will be derived in 2-D in order to alleviate the notation, although the 3-D derivation is analogous. Let $u^{(s)} \triangleq u^{(s)}(x,y,t)$ be the concentration of species s, $\bar{u}_{\mathbf{i}}^{(s)}$ be the average concentration at volume element $\mathbf{i}$, to wit $\bar{u}_{\mathbf{i}}^{(s)} \triangleq h^{-2}\int_{\mathbf{i}} u^{(s)}\mathrm{d}V$, where h is the length of element $\mathbf{i}$, and $U_{\mathbf{i}}^{(s)}$ denotes the number of molecules in a volume element, videlicet $U_{\mathbf{i}}^{(s)} \triangleq \int_{\mathbf{i}} \bar{u}_{\mathbf{i}}^{(s)}\mathrm{d}V = \bar{u}_{\mathbf{i}}^{(s)}h^2$. It can be shown that an infinite number of molecules that are subject to Brownian motion is equivalent to the continuum diffusion equation [5]. The diffusion equation consists of the equations for the conservation of mass

$$\frac{\partial u^{(s)}}{\partial t} = -\nabla\cdot\mathbf{J}, \tag{7}$$

and Fick's law for the flux $\mathbf{J}$:

$$\mathbf{J} = -D^{(s)}\nabla u^{(s)}, \tag{8}$$

where $D^{(s)}$ is the macroscopic diffusion coefficient of the species s. It is assumed that $D^{(s)}$ is constant throughout this derivation, although this need not be the case. It has been shown in [30,31] that spatially-dependent diffusion coefficients can be used with finite volume schemes. Specifically, the harmonic average is used to determine the diffusion coefficient across interfaces.

Integrating Eq. (7) over a volume element $\mathbf{i}$ and applying the divergence theorem on the right-hand-side yields

$$\frac{\mathrm{d}U_{\mathbf{i}}^{(s)}}{\mathrm{d}t} = -\oint_{\partial\mathbf{i}} \mathbf{J}\cdot\mathbf{n}\,\mathrm{d}S. \tag{9}$$

Decomposing the surface integral into faces, γ_a, $a = 1,\ldots,4$, gives [10]

$$\frac{\mathrm{d}U_{\mathbf{i}}^{(s)}}{\mathrm{d}t} = -\sum_{a=1}^{4}\int_{\gamma_a} \mathbf{J}\cdot\mathbf{n}\,\mathrm{d}S. \tag{10}$$

2.1. Uniform mesh interfaces

The flux $\mathbf{J}$ between neighboring volume elements that have the same length, i.e. not at an interface, is obtained by virtue of a centered second-order finite-difference scheme (see Fig. 1). For the face γ_1, the flux is

$$\mathbf{J}\left(x-\frac{h}{2},y\right) = -D^{(s)}\left(\frac{\bar{u}_{\mathbf{l}}^{(s)}-\bar{u}_{\mathbf{i}}^{(s)}}{h}\right)+\mathcal{O}(h^2). \tag{11}$$

Employing a quadrature on the interface and substituting $U_{\mathbf{i}}^{(s)}$ for $\bar{u}_{\mathbf{i}}^{(s)}$ yields

$$\frac{\mathrm{d}U_{\mathbf{i}}^{(s)}}{\mathrm{d}t} = -\int_{\gamma_1}\mathbf{J}\left(x-\frac{h}{2},y\right)\cdot\mathbf{n}\,\mathrm{d}S = D^{(s)}\left(\frac{\bar{u}_{\mathbf{l}}^{(s)}-\bar{u}_{\mathbf{i}}^{(s)}}{h}\right)h+\mathcal{O}(h^2) = \frac{D^{(s)}}{h^2}\left(U_{\mathbf{l}}^{(s)}-U_{\mathbf{i}}^{(s)}\right)+\mathcal{O}(h^2). \tag{12}$$

The diffusion propensities are the rates per unit time [10]:

$$a_{\mathbf{i},\mathbf{l}}^{(s)} = \frac{D^{(s)}}{h^2}U_{\mathbf{l}}^{(s)}, \tag{13}$$

$$a_{\mathbf{l},\mathbf{i}}^{(s)} = \frac{D^{(s)}}{h^2}U_{\mathbf{i}}^{(s)}, \tag{14}$$

where these represent the unscaled probabilities of a molecule that moves from volume element $\mathbf{l}$ to $\mathbf{i}$ and vice versa, respectively.

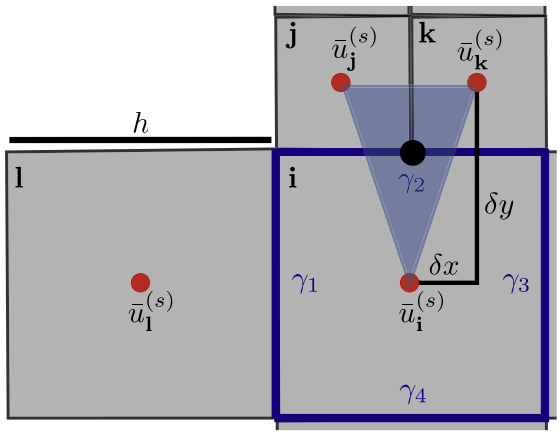

Fig. 1. Stencil for the adaptive multiresolution mesh. Taylor's series are used to determine the flux across the interface formed by volume elements **i**, **j**, and **k**. The flux along the *y*-axis is approximated at the point depicted as • in the triangle.

2.2. Locally refined mesh interfaces

For coarse–fine interfaces, series expansions will be used to approximate the gradient by fitting a plane through the known values, e.g. cells **i**, **j** and **k** across the interface γ_2 in Fig. 1. Three second-order Taylor's series will be used to approximate $\mathbf{J}(x,\ y+\frac{2}{3}\delta y)$, namely: $\bar{u}_{\mathbf{i}}^{(s)},\ \bar{u}_{\mathbf{j}}^{(s)}$, and $\bar{u}_{\mathbf{k}}^{(s)}$ about the point $(x, y+\frac{2}{3}\delta y)$:

$$\bar{u}_{\mathbf{i}}^{(s)} = u^{(s)}\left(x, y+\frac{2}{3}\delta y\right) - \frac{2\delta y}{3}\frac{\partial}{\partial y}u^{(s)}\left(x, y+\frac{2}{3}\delta y\right) + \mathcal{O}(h^2), \tag{15}$$

$$\bar{u}_{\mathbf{j}}^{(s)} = u^{(s)}\left(x, y+\frac{2}{3}\delta y\right) - \delta x\frac{\partial}{\partial x}u^{(s)}\left(x, y+\frac{2}{3}\delta y\right) + \frac{\delta y}{3}\frac{\partial}{\partial y}u^{(s)}\left(x, y+\frac{2}{3}\delta y\right) + \mathcal{O}(h^2), \tag{16}$$

$$\bar{u}_{\mathbf{k}}^{(s)} = u^{(s)}\left(x, y+\frac{2}{3}\delta y\right) + \delta x\frac{\partial}{\partial x}u^{(s)}\left(x, y+\frac{2}{3}\delta y\right) + \frac{\delta y}{3}\frac{\partial}{\partial y}u^{(s)}\left(x, y+\frac{2}{3}\delta y\right) + \mathcal{O}(h^2), \tag{17}$$

where $\delta x \triangleq h/4$ and $\delta y \triangleq 3h/4$.

Multiplying Eq. (15) by two and subtracting Eqs. (16) and (17) gives

$$-2\delta y\frac{\partial}{\partial y}u^{(s)}\left(x, y+\frac{2}{3}\delta y\right) = 2\bar{u}_{\mathbf{i}}^{(s)} - \bar{u}_{\mathbf{j}}^{(s)} - \bar{u}_{\mathbf{k}}^{(s)} + \mathcal{O}(h^2). \tag{18}$$

Isolating the derivative along the *y*-axis requires dividing by δy and renders the approximation first-order:

$$\frac{\partial}{\partial y}u^{(s)}\left(x, y+\frac{2}{3}\delta y\right) = \frac{1}{2\delta y}\left(\bar{u}_{\mathbf{j}}^{(s)} + \bar{u}_{\mathbf{k}}^{(s)} - 2\bar{u}_{\mathbf{i}}^{(s)}\right) + \mathcal{O}(h). \tag{19}$$

The flux for the cell averages is therefore

$$\mathbf{J}\left(x, y+\frac{2}{3}\delta y\right) = -\frac{D^{(s)}}{2\delta y}\left(\bar{u}_{\mathbf{j}}^{(s)} + \bar{u}_{\mathbf{k}}^{(s)} - 2\bar{u}_{\mathbf{i}}^{(s)}\right) + \mathcal{O}(h). \tag{20}$$

Using a quadrature, substituting in h for δy, $U_{\mathbf{i}}^{(s)}$ for $\bar{u}_{\mathbf{i}}^{(s)}$ and analogously for $\bar{u}_{\mathbf{j}}^{(s)}$ and $\bar{u}_{\mathbf{k}}^{(s)}$, and simplifying yields the following difference equation across the interface:

$$\frac{\mathrm{d}U_{\mathbf{i}}^{(s)}}{\mathrm{d}t} = -\int_{\gamma_2}\mathbf{J}\left(x, y+\frac{2}{3}\delta y\right)\cdot\mathbf{n}\ \mathrm{d}S = \frac{4D^{(s)}}{3h^2}\left(2\left(U_{\mathbf{j}}^{(s)} + U_{\mathbf{k}}^{(s)}\right) - U_{\mathbf{i}}^{(s)}\right) + \mathcal{O}(h). \tag{21}$$

The derivations for the fine volume elements, *j* and *k*, use the fluxes

$$\mathbf{J}\left(x \pm \delta x, y+\frac{2}{3}\delta y\right) = \mathbf{J}\left(x, y+\frac{2}{3}\delta y\right), \tag{22}$$

which result in

$$\frac{\mathrm{d}U_{\mathbf{j}}^{(s)}}{\mathrm{d}t} = \frac{\mathrm{d}U_{\mathbf{k}}^{(s)}}{\mathrm{d}t} = \frac{2D^{(s)}}{3h^2}\left(U_{\mathbf{i}}^{(s)} - 2\left(U_{\mathbf{j}}^{(s)} + U_{\mathbf{k}}^{(s)}\right)\right) + \mathcal{O}(h), \tag{23}$$

where the quadratures are performed with an interface length of $h/2$. Additionally, the following conservative requirement across the interface is satisfied:

$$\frac{dU_{\mathbf{i}}^{(s)}}{dt} = -\left(\frac{dU_{\mathbf{j}}^{(s)}}{dt} + \frac{dU_{\mathbf{k}}^{(s)}}{dt}\right). \tag{24}$$

Analogously to the propensities defined in Eqs. (13) and (14), the propensities across the interface are

$$a_{\mathbf{i},\mathbf{j}}^{(s)} = a_{\mathbf{i},\mathbf{k}}^{(s)} = \frac{4D^{(s)}}{3h^2}\left(U_{\mathbf{j}}^{(s)} + U_{\mathbf{k}}^{(s)}\right), \tag{25}$$

$$a_{\mathbf{j},\mathbf{i}}^{(s)} = a_{\mathbf{k},\mathbf{i}}^{(s)} = \frac{2D^{(s)}}{3h^2}U_{\mathbf{i}}^{(s)}. \tag{26}$$

3. Reactions and the homogeneity condition

The reaction propensities depend only on the number of each species in each volume element. A reaction m in volume element $\mathbf{i}$ can be written as

$$\sum_s r^{(s)}U_{\mathbf{i}}^{(s)} \xrightarrow{k_+} \sum_s g^{(s)}U_{\mathbf{i}}^{(s)}, \tag{27}$$

where k_+ is related to the cross-section of a collision of the required molecules [15]; $r^{(s)}$ and $g^{(s)}$ are the numbers of reactants and products of species s, respectively. The propensity is defined as

$$a_{\mathbf{i}}^{(m)} = \Omega_{\mathbf{i}}k_+\prod_s\left\{\frac{\left(\left(U_{\mathbf{i}}^{(s)}\right)\right)^{r^{(s)}}}{\Omega_{\mathbf{i}}^{r^{(s)}}}\right\}, \tag{28}$$

where $\left(\left(U_{\mathbf{i}}^{(s)}\right)\right)^{r^{(s)}} \triangleq U_{\mathbf{i}}^{(s)}\left(U_{\mathbf{i}}^{(s)}-1\right)\left(U_{\mathbf{i}}^{(s)}-2\right)\cdots\left(U_{\mathbf{i}}^{(s)}-r^{(s)}+1\right)$. The validity of Eq. (28) rests on the assumption that the volume element $\mathbf{i}$ is homogeneous. This condition has been shown to be equivalent to [6]

$$\frac{\tau_R}{\tau_D} \gg 1, \tag{29}$$

where τ_R is the mean free time with respect to reactive collisions in a volume element and τ_D is the mean time during which a molecule will remain in a volume element. An estimate of this ratio for a bimolecular reaction, irrespective of the dimensionality of the problem, is given by [11]

$$\frac{\hat{\tau}_R}{\hat{\tau}_D} = \frac{D}{h^2k_+}, \tag{30}$$

which shows that fine spatial resolutions are necessary to enforce the homogeneity condition. It should be noted that there is a lower-bound on the size of the volume elements (see [9,27,32]). In this work, however, the refinement procedure is halted after a predefined number of levels has been reached.

4. Adaptivity

4.1. Refinement criterion

At every predefined number of iterations in the simulation algorithm, all of the refined levels are coarsened to the top level. Since the volume elements represent the number of molecules of a species and the refinement ratio is constant, the four (2-D) or eight (3-D) values are summed to produce the value at the next coarsest level.

Let $\boldsymbol{\alpha}$, $\boldsymbol{\beta}$, $\boldsymbol{\gamma}$, and $\boldsymbol{\delta}$ denote the indices of the neighboring cells of element $\mathbf{i}$. The refinement criterion follows directly from the homogeneity assumption in that the objective is to minimize the gradients between volume elements. If the system were in equilibrium, the value of $U_{\boldsymbol{\alpha}}^{(s)}$ can be approximated by $U_{\boldsymbol{\alpha}}^{(s)} \sim \mathcal{N}(\Omega,\Omega)$, where the volume element indices for Ω have been discarded since the values are on the same level and $\mathcal{N}(\mu,\sigma^2)$ denotes the Gaussian distribution with mean μ and variance σ^2. The values of $U_{\boldsymbol{\alpha}}^{(s)}$ are expected to be between $\Omega - C\sqrt{\Omega}$ and $\Omega + C\sqrt{\Omega}$ with probability equal to $\mathrm{erf}(C/\sqrt{2})$, which is $\approx$0.997 if $C = 3$. Therefore,

$$p\left(U_{\boldsymbol{\alpha}}^{(s)} \notin \left[\Omega - C\sqrt{\Omega}, \Omega + C\sqrt{\Omega}\right]\right) = 1 - \mathrm{erf}(C/\sqrt{2}) = \mathrm{erfc}(C/\sqrt{2}). \tag{31}$$

To illustrate the method, the one-dimensional case will be considered as shown in Fig. 2. Following Bell et al. [4], a volume element $\mathbf{i}$ is refined if

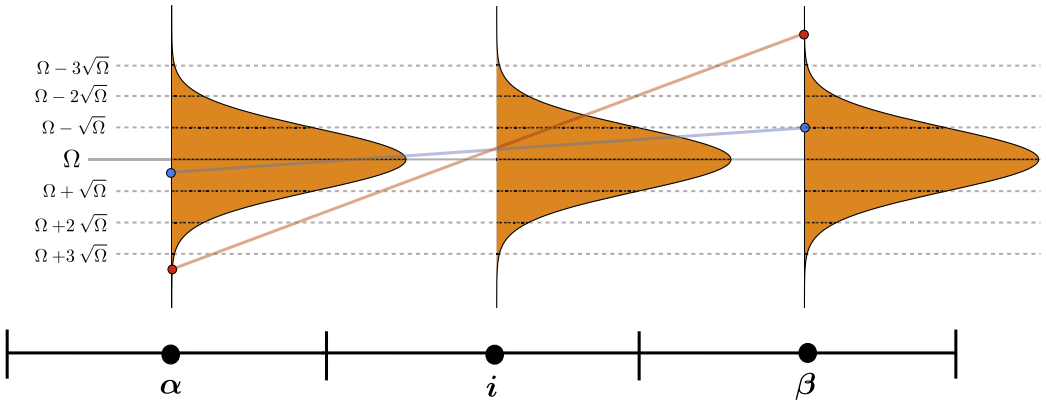

Fig. 2. Schematic of the refinement criterion. Shown in orange are Gaussian distributions with mean and variance Ω. The criterion distinguishes between small gradients arising because of fluctuations and large gradients arising from the physics of the problem (see [4]). The dashed black lines denote the mean plus/minus the standard deviations. (For interpretation of the references to colour in this figure legend, the reader is referred to the web version of this article.)

$$\left|U_{\beta}^{(s)} - U_{\alpha}^{(s)}\right| > 2C\sqrt{\Omega}, \tag{32}$$

which will ensure that there are indeed gradients and not fluctuations. In this work, a specific species was monitored although this need not be the case. The value of C dictates how sensitive the criterion is to gradients. A low value of C would result in refinement in many regions, even with small or nonexistent gradients, and thus decrease the overall error of the diffusion process. Therefore, the value of C is related to the discretization error, where $C = 3$ has been used throughout this work. In terms of the errors defined in Eq. (6), $C_3 \sim C$. In two dimensions, the maximum of the gradients will be used, i.e. a volume element $\mathbf{i}$ is refined if

$$\max\left(\left|U_{\beta}^{(s)} - U_{\alpha}^{(s)}\right|, \left|U_{\delta}^{(s)} - U_{\gamma}^{(s)}\right|\right) > 2C\sqrt{\Omega}. \tag{33}$$

We note that the gradient is computed on the coarsest mesh level, which provides an implicit filtering operation. We find that this refinement criterion was adequate in the two numerical examples that are considered in Section 5 considered. This does not necessarily imply that this is the best possible criterion but perhaps a good first choice. Indeed in certain cases, due to noisy gradient evaluation, the gradient algorithm led to spurious mesh refinement. However, for the Fisher–Kolmogorov and Gray–Scott problems considered in this paper, the gradient-based refinement criterion was adequate. It should be noted that problems in which small scales appear owing to the curvature of the field instead of the gradient, this criterion will fail to tag the proper volume elements for refinement.

4.2. Stochastic interpolation

The values of the new volume elements that did not exist in the previous iteration are determined by first analyzing the equilibrium case, which are known to be Poisson distributed random variables. Given that the coarse value is $U_{\mathbf{i}}^{(s)}$, four (2-D) or eight (3-D) values, $\widehat{U}_1^{(s)}, \ldots$, need to be determined. A multinomial distribution, which enforces that every volume element is Poisson distributed according to the size of the volume element, can be written as

$$\widehat{U}_i^{(s)} \sim \mathcal{B}\left(U_{\mathbf{i}}^{(s)} - \sum_{j=1}^{i-1} \widehat{U}_j^{(s)}, \frac{\hat{p}_i}{1 - \sum_{j=1}^{i-1} \hat{p}_j}\right), \tag{34}$$

for $i = 1, \ldots, 4$ (2-D), where $\hat{p}_i$ are weights that can be determined by interpolation. In equilibrium, the interpolation scheme is exact, and the weights are 1/4 (2-D) or 1/8 (3-D). In the non-equilibrium case, interpolation was used to determine the weights. The result is a scheme that is strictly positive and conservative. In terms of the error, the scheme is $\mathcal{O}(h^2)$ with respect to the first moment of the field. The weights, which are determined by a tensor product of 1-D weights, are

$$\hat{p}_1 = Z^{-1}\phi_1\phi_2, \tag{35}$$
$$\hat{p}_2 = Z^{-1}\phi_1\phi_4, \tag{36}$$
$$\hat{p}_3 = Z^{-1}\phi_3\phi_2, \tag{37}$$
$$\hat{p}_4 = Z^{-1}\phi_3\phi_4, \tag{38}$$

where $Z = 64\left(U_{\alpha}^{(s)} + U_{\beta}^{(s)}\right)\left(U_{\gamma}^{(s)} + U_{\delta}^{(s)}\right)$, $\phi_1 = \left(5U_{\alpha}^{(s)} + 3U_{\beta}^{(s)}\right)$, $\phi_2 = \left(5U_{\gamma}^{(s)} + 3U_{\delta}^{(s)}\right)$, $\phi_3 = \left(3U_{\alpha}^{(s)} + 5U_{\beta}^{(s)}\right)$, $\phi_4 = \left(3U_{\gamma}^{(s)} + 5U_{\delta}^{(s)}\right)$, and $U_{\alpha}^{(s)}, \ldots, U_{\delta}^{(s)}$ are the neighboring volume elements as shown in Fig. 3.

5. Numerical results

5.1. Validation

The numerical method is validated by verifying that (i) Eqs. (12), (21) and (23) converge to the solution of the heat equation and (ii) the propensities defined in Eqs. (13), (14), (25) and (26) – by virtue of Eqs. (12), (21) and (23) – reproduce the distributions associated with a random walk.

5.1.1. Convergence

Eqs. 12, 21 and 23 govern the stochastic diffusion process, and can be integrated using the aforementioned stochastic simulation algorithms (Eqs. (2)–(5)). In the limit of an infinite number of molecules, it can be shown that stochastic simulation algorithms tend to the deterministic reaction rate equations [15,29]. Invoking this limit will facilitate the analysis of convergence with respect to Eqs. (12), (21) and (23).

A convergence analysis of Eqs. (12), (21) and (23) was performed using the following function for the initial condition: $u_{initial}(x,y) = \sin(\pi x)\sin(\pi y)$, $x,y \in [0,1] \times [0,1]$ for a uniform mesh and a composite mesh that included a refined region in the center of the domain, i.e. in $[0.3,0.7] \times [0.3,0.7]$. Simulations were performed with the explicit Euler method in $t \in [0,5 \cdot 10^{-2}]$ using homogeneous Dirichlet boundary conditions such that 60% of the initial function decayed. The time-step was chosen in accordance with the stability restriction of the explicit Euler method, namely

$$\Delta t = \frac{\mathcal{F}_o C_3 h_{\min}^2}{\max_s(D^{(s)})} \tag{39}$$

where $C_3 < 1$, $D^{(s)} = 1$ here, and $\mathcal{F}_o = 1/(2d)$ is the so-called Fourier number, where d is the dimension of the problem. Fig. 4 reveals that the composite mesh had a lower relative L_2 error, and, although the local errors of Eqs. (21) and (23) are formally

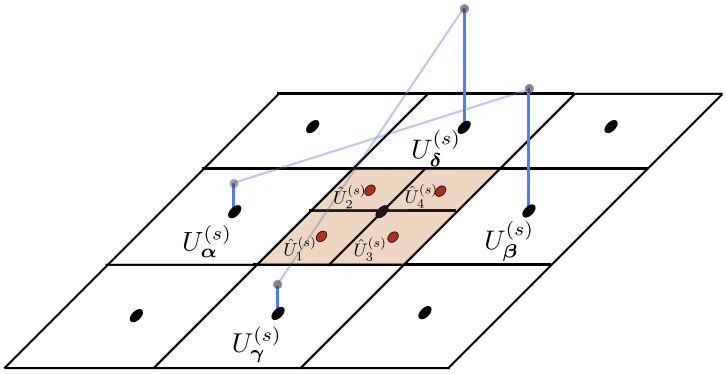

Fig. 3. Stochastic interpolation for refined volume elements: the shaded region represents the volume element that is tagged for refinement. The values for the new volume elements, $\hat{U}_1^{(s)}, \ldots, \hat{U}_4^{(s)}$, are sampled from a multinomial distribution. The weights for the distribution are determined from a strictly positive and conservative interpolation using the four neighboring values.

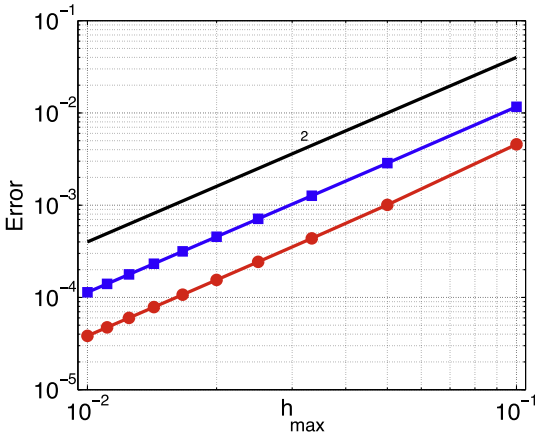

Fig. 4. Relative L_2 error versus the maximum volume element length for simulations of the diffusion equation. Uniform mesh, ▪, and a composite mesh that contained a coarse and fine mesh, ·.

first-order, global second-order convergence is achieved. This phenomenon is indicative of *supraconvergence*, which is an increase in the rate of convergence of finite volume approximations based on conservation laws [10,33].

5.1.2. Fluctuations in equilibrium

The values $U_{\mathbf{i}}^{(s)}$ in equilibrium are, theoretically, Poisson distributed, videlicet [6]: $U_{\mathbf{i}}^{(s)} \sim \mathcal{P}(\Omega_{\mathbf{i}})$, where $\Omega_{\mathbf{i}} \triangleq Q\,\delta V_{\mathbf{i}}$ such that Q is a constant that represents the total number of molecules in a volume element at the coarsest level and $\delta V_{\mathbf{i}}$ is the relative size of the volume element $\mathbf{i}$. Stochastic diffusion was simulated in equilibrium with $Q = 960$ using a 3-level composite mesh that consisted of one mesh per level. Shown in Fig. 5 are discrete probability density functions for three cells that were located in the bulk, at the interface, and at a corner of each of the two refined meshes. A slight departure from the correct distribution can be seen for the cells that lie on the interface between two different sized meshes as suggested by the aforementioned error analysis.

5.2. Numerical examples

5.2.1. Fisher–Kolmogorov model

The Fisher–Kolmogorov equation, which was proposed as a model for the spatial propagation of an advantageous gene in a population, is [25]

$$\frac{\partial u^{(1)}}{\partial t} - D^{(1)}\Delta u^{(1)} = \lambda u^{(1)}u^{(2)}, \tag{40}$$

$$= \lambda u^{(1)}(1 - u^{(1)}), \tag{41}$$

where $u^{(s)} = u^{(s)}(x,t)$. In Eq. (41), the conservation relation $u^{(1)} + u^{(2)} = 1$ has been used to eliminate $u^{(2)}$. An analytical solution can be derived in 1-dimension [34]:

$$u^{(1)}(z) = \frac{1}{(1 + ae^{bz})^2}, \tag{42}$$

where $z = x - ct,\ a = \sqrt{2} - 1,\ b = 80\sqrt{2/3}$, and the wavespeed $c = \frac{5}{\sqrt{6}}\sqrt{D^{(1)}\lambda} = 1/(32\sqrt{6})$. The discrete model takes the form

$$U_{\mathbf{i}}^{(1)} + U_{\mathbf{i}}^{(2)} \xrightarrow{\lambda} 2U_{\mathbf{i}}^{(1)}, \tag{43}$$

where $U_{\mathbf{i}}^{(1)}$ and $U_{\mathbf{i}}^{(2)}$ are both diffusive species with the same diffusion coefficient $D^{(1)}$. This system was simulated stochastically using the τ-Leaping [35] algorithm in a unit square using the present adaptive multiresoltuion method with $D^{(1)} = 1/160^2$, $\lambda = 1$, $h_{min} = 1/800$, $h_{max} = 1/100$, $C = 3$, and $\hat{\tau}_R/\hat{\tau}_D = 25$ using the following initial condition:

$$U_{\mathbf{i}}^{(1)} = \left\lceil \frac{\Omega_{\mathbf{i}}}{(1 + ae^{b(\|\mathbf{x}_{\mathbf{i}} - \mathbf{c}\| - r)})^2} \right\rfloor, \tag{44}$$

where $\mathbf{x}_{\mathbf{i}}$ is the center of volume element i, $\mathbf{c} = (1/2, 1/2)^T$, $r = 1/5$, $\lceil\cdot\rfloor$ denotes the rounding operator, $Q = 960$, and again $\Omega_{\mathbf{i}} \triangleq Q\delta\ V_{\mathbf{i}}$, which means that the number of molecules at the finest level is on the order of 15. $U_{\mathbf{i}}^{(2)}$ is defined as the complement of $U_{\mathbf{i}}^{(1)}$ such that $U_{\mathbf{i}}^{(1)} + U_{\mathbf{i}}^{(2)} = \Omega_{\mathbf{i}}$. A simulation was performed in $t \in [0,20]$, the results of which are shown in Figs. 6 and 7. On the right panel in Fig. 6, a disk is shown that expands with a speed of c per unit time. The numerical wavespeed

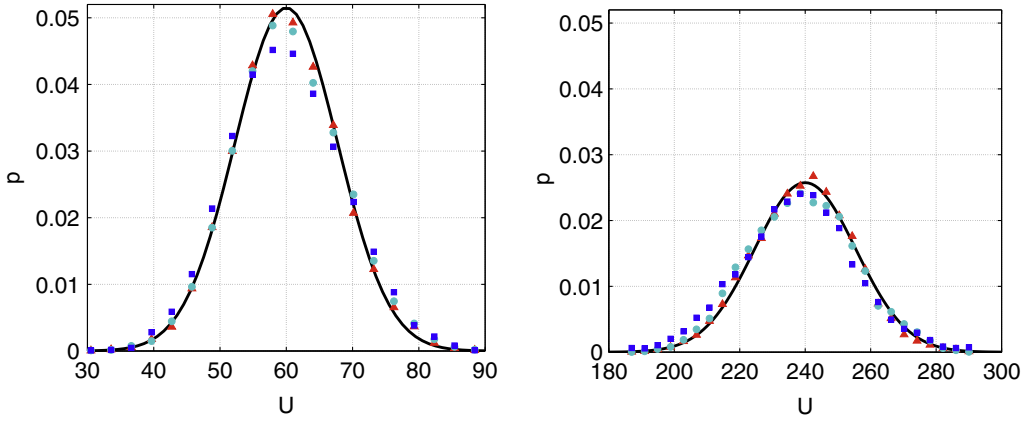

Fig. 5. Discrete probability density functions for stochastic diffusion in equilibrium for a 3-level composite mesh: level 3 (left) and level 2 (right) are shown using a cell from the bulk ▲, from the interface ●, and from a corner ■ of each of the two refined meshes. The black lines correspond to the Gaussian distribution.

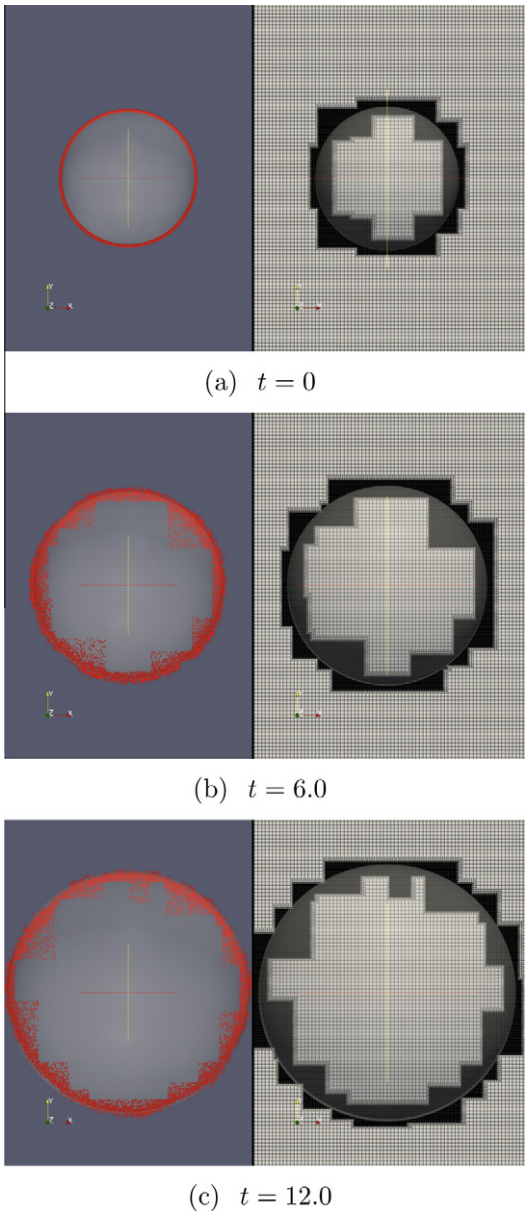

Fig. 6. Stochastic simulation of the Fisher–Kolmogorov propagating front at various times. The left panel shows the concentration of $U_i^{(1)} \in [0.45, 0.55]$ as ●, and the right panel depicts the adaptive multiresolution mesh and a radial projection the 1-D solution for reference (white circle).

for the 2-D problem is $0.9436c$ as shown in Fig. 8(a). Additionally, the position of the front with respect to the angle at time $t = 6$ is shown in Fig. 8(b). The contour value 1/5 was used for both panels of Fig. 8.

5.2.2. Gray–Scott model

The *Gray–Scott* model is an example of self-organization in non-equilibrium, chemically reacting systems [26]. The partial differential equations for this model are

$$\frac{\partial u^{(1)}}{\partial t} - D^{(1)}\Delta u^{(1)} = -\rho u^{(1)}{u^{(2)}}^2 + F(1 - u^{(1)}), \tag{45}$$

$$\frac{\partial u^{(2)}}{\partial t} - D^{(2)}\Delta u^{(2)} = \rho u^{(1)}{u^{(2)}}^2 - (F + \kappa)u^{(2)}. \tag{46}$$

The following chemical reactions represent the discrete model:

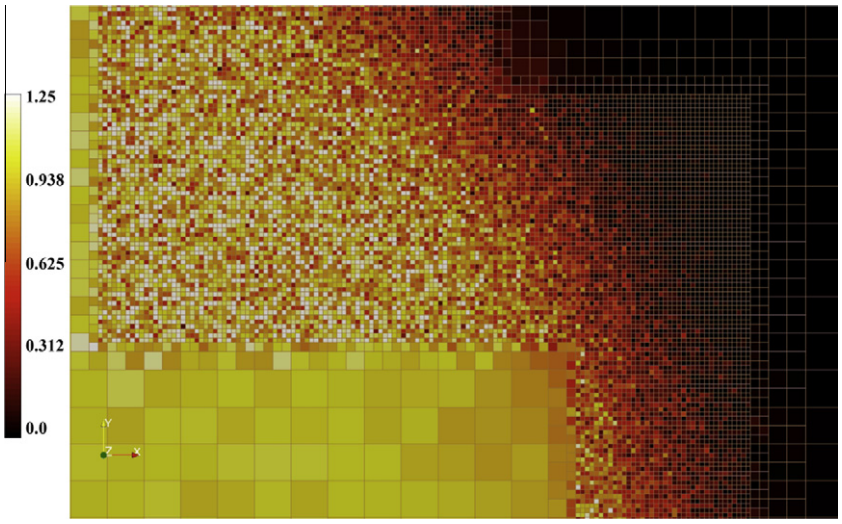

Fig. 7. Enlargement of a region of the domain for the concentration of $U_{\mathbf{i}}^{(1)}$ at time $t = 6.0$ for a stochastic simulation of the Fisher–Kolmogorov front.

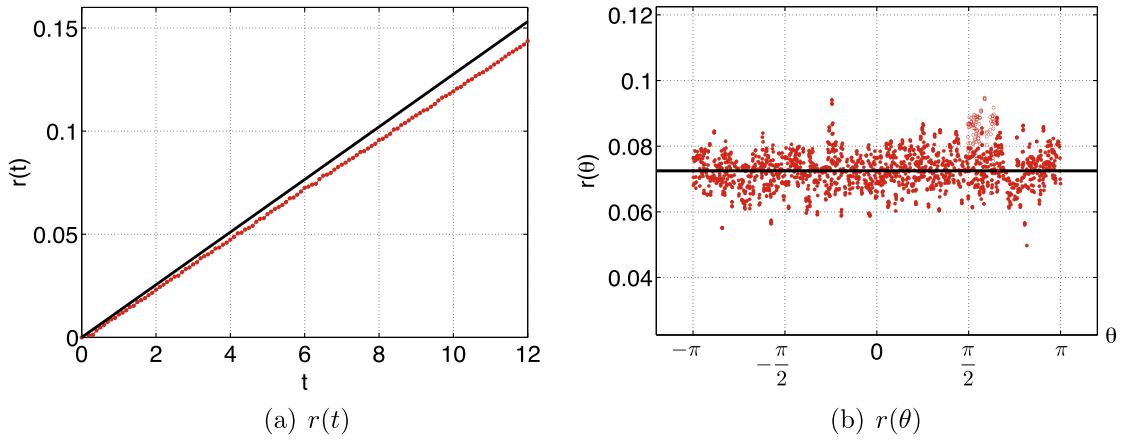

Fig. 8. Analysis of simulation of the Fisher–Kolmogorov propagating front. The left panel (a) shows the concentration of mean radius of the propagating front over time, $r(t)$, where · is the numerical value averaged over all angles θ and the black line is the 1-D analytically-derived wavespeed. The right panel (b) depicts values with respect to θ at time $t = 6$ as ●, where the black line is the mean value.

$$U_{\mathbf{i}}^{(1)} + 2U_{\mathbf{i}}^{(2)} \xrightarrow{\rho} 3U_{\mathbf{i}}^{(2)}, \tag{47}$$

$$\emptyset \xrightarrow{F} U_{\mathbf{i}}^{(1)}, \tag{48}$$

$$U_{\mathbf{i}}^{(1)} \xrightarrow{F} \emptyset, \tag{49}$$

$$U_{\mathbf{i}}^{(2)} \xrightarrow{F+\kappa} \emptyset. \tag{50}$$

The initial conditions for the two species are

$$U_{\mathbf{i}}^{(1)} = \begin{cases} \left[\Omega_{\mathbf{i}}\left(\frac{1}{2} + \xi \cdot 10^{-2}\right)\right] & \text{if } \mathbf{x}_{\mathbf{i}} \in \mathcal{G}_{\text{int}} \\ \left[\Omega_{\mathbf{i}}(1 + \xi \cdot 10^{-2})\right] & \text{otherwise} \end{cases}, \tag{51}$$

$$U_{\mathbf{i}}^{(2)} = \begin{cases} \left[\Omega_{\mathbf{i}}\left(\frac{1}{4} + \xi \cdot 10^{-2}\right)\right] & \text{if } \mathbf{x}_{\mathbf{i}} \in \mathcal{G}_{\text{int}} \\ \left[\Omega_{\mathbf{i}}(\xi \cdot 10^{-2})\right] & \text{otherwise} \end{cases}, \tag{52}$$

where $\xi \sim \mathcal{U}(0,1)$ and $\mathcal{G}_{\text{int}} = [1/4, 3/4] \times [1/4, 3/4]$. Fig. 9 shows the concentration of $U_{\mathbf{i}}^{(1)}$ along with mesh at various times for a simulation using the τ-Leaping [35] algorithm in a unit square domain, where $t \in [0, 1000]$, $\rho = 1$, $F = 2.8 \cdot 10^{-2}$,

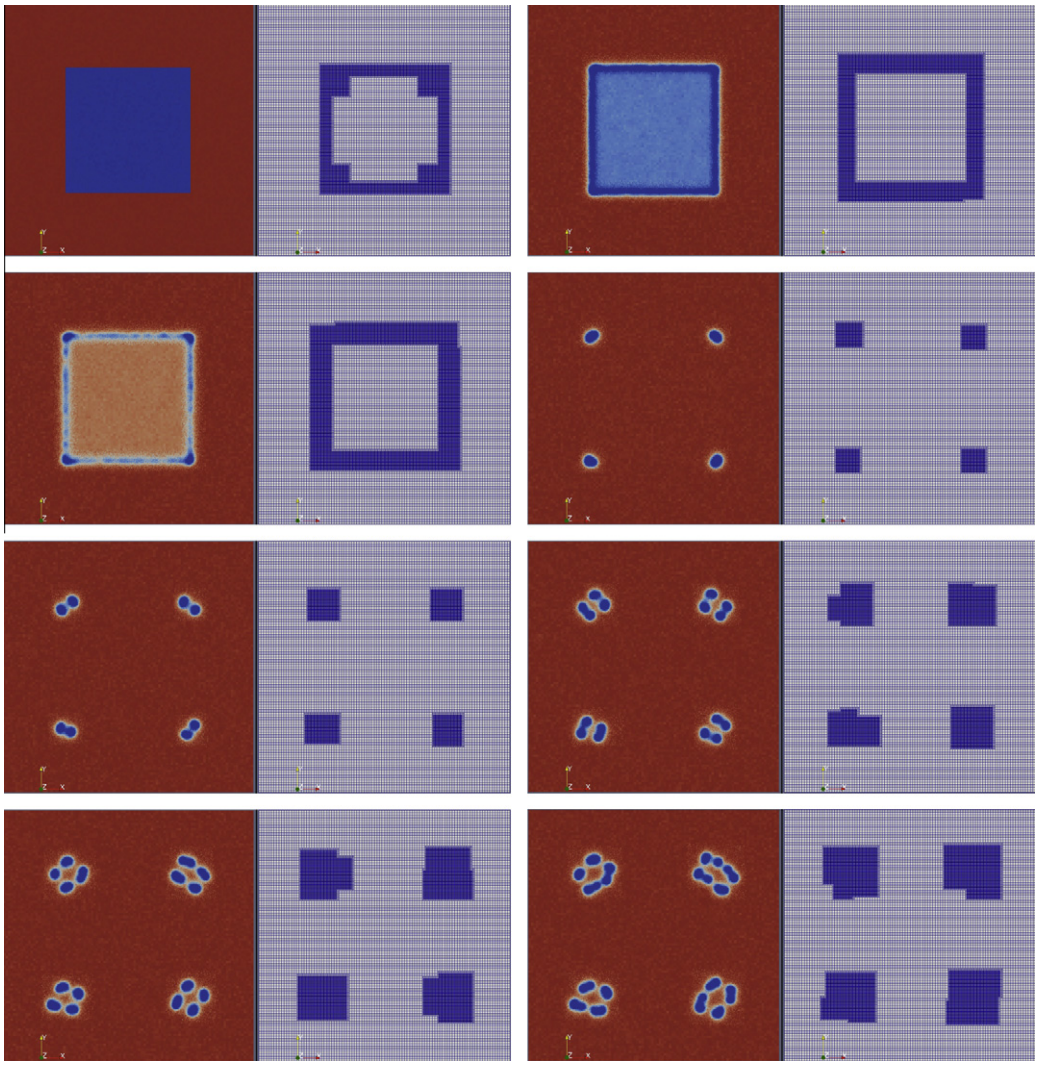

Fig. 9. Stochastic simulation of the Gray–Scott model at various times with the adaptive mesh (left to right, top to bottom): $t = 0,75, 115, 255, 435, 700, 870, 1000$.

$\kappa = 6.1 \cdot 10^{-2}$, $D^{(1)} = 12.5 \cdot 10^{-5}$, $D^{(2)} = 6.25 \cdot 10^{-5}$, $C = 3$, and $Q = 10^4$, which results in 625 molecules at the finest level if the concentration is 1. The species $U_i^{(1)}$ was used to monitor the gradient in Eq. (33). The resolution of the simulation was $h_{min} = 1/400$ and $h_{max} = 1/100$. Although the stochastic simulation of the Gray-Scott equations was qualitatively similar to a deterministic simulation, the symmetry is not necessarily preserved as shown in Fig. 10.

5.2.3. Implementation

The code has been written in C++ and made use of the AMR methods and data-structures in the **Overture** library [36,37]. The time-integration method that was used was τ-Leaping [35] in order to have explicit control over the time-step. Specifically, the time-step is chosen such that it obeys the stability condition imposed by the diffusion process, namely Eq. (39). This was done since the error control parameter, ϵ, does not necessarily enforce stability. Additionally, since the diffusion propensities should be larger than the reactions propensities due to local homogeneity (see Section 3), it is reasonable to impose a bound on the diffusion process. It should be noted that the methods developed here are independent of the time-integration scheme and therefore can be combined with other stochastic simulation algorithms [18].

The running time for a d dimensional spatially-dependent simulation is $\mathcal{O}(L)$, where $L = h^{-d}$, $h = 1/N_e$, and N_e is the number of elements per dimension. In other words, L is the total number of volume elements in the simulation. The objective of using adaptive mesh refinement can be seen as either (i) reducing the error of a simulation by effectively introducing more volume elements into regions of the domain where the error is expected to be the largest (e.g. regions where the gradients are large) whilst keeping the running time essentially constant or (ii) minimizing the number of volume elements so as to reduce the

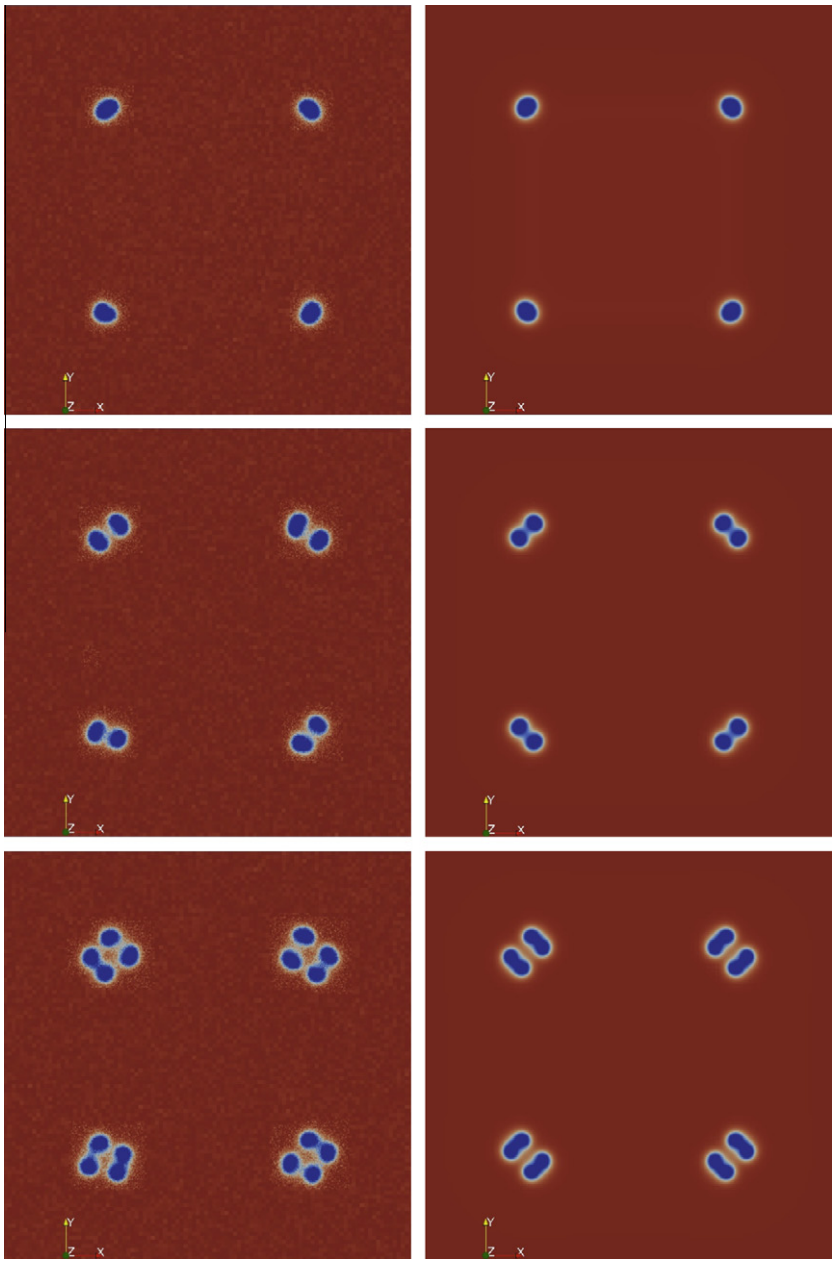

Fig. 10. Comparison of stochastic (left column) and deterministic (right column) multiresolution simulations of the Gray–Scott equations. Time from top to bottom: $t = 250, 500, 750$.

running time of the simulation whilst keeping the error essentially constant. Assuming that the objective is (ii), a computational efficiency variable can be defined as

$$E(t) = \frac{L_{amr}(t)}{L_{h_{min}}}, \tag{53}$$

where $L_{amr}(t)$ is the number of volume elements in the simulation at time t and $L_{h_{min}}$ is the number of volume elements under the assumption that h_{min} is used throughout the domain. The values of $L_{h_{min}}$ are 800^2 and 400^2 for the Fisher–Kolmogorov (Section 5.2.1) and Gray–Scott (Section 5.2.2) problems, respectively. A value of $E(t) = 1$ describes the situation in which all of the volume elements are refined to the finest level. Fig. 11 shows the efficiency of the two model problems considered in this work.

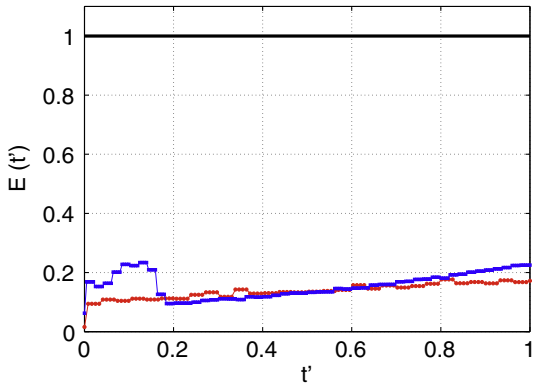

Fig. 11. Efficiency of Fisher–Kolmogorov and Gray–Scott simulations. The value $E(t')$, which is a measure of computational efficiency, is shown for the Fisher–Kolmogorov · and Gray–Scott problems ▪. The time axis has been rescaled to be in the interval $t' \in [0,1]$ for both problems.

6. Conclusion

A spatially adaptive simulation method for the reaction–diffusion master equation has been presented. The diffusion rates on locally refined meshes have been derived and validated. Furthermore, refinement and coarsening criteria and a stochastic interpolation scheme have been proposed for stochastic simulations based on adaptive mesh refinement. The method was shown to be useful for problems that exhibit a localization of spatial scales such as in wave propagation and pattern formation processes.

The proposed method should be profitable in intracellular biochemical modeling since cells often have a low copy number of reactive molecules that undergo diffusion.

Acknowledgements

The authors thank Francesco Miniati at ETH Zurich for a helpful discussion regarding AMR.

References

[1] M.J. Berger, J. Oliger, Adaptive mesh refinement for hyperbolic partial differential equations, J. Comput. Phys. 53 (3) (1984) 484–512.
[2] M.J. Berger, P. Colella, Local adaptive mesh refinement for shock hydrodynamics, J. Comput. Phys. 82 (1) (1989) 64–84.
[3] A.L. Garcia, J.B. Bell, W.Y. Crutchfield, B.J. Alder, Adaptive mesh and algorithm refinement using direct simulation Monte Carlo, J. Comput. Phys. 154 (1) (1999) 134–155.
[4] A.L. Garcia, J.B. Bell, J. Foo, Algorithm refinement for the stochastic burgers' equation, J. Comput. Phys. 223 (1) (2007) 451–468.
[5] S. Chandrasekhar, Stochastic problems in physics and astronomy, Rev. Mod. Phys. 15 (1) (1943) 0001–0089.
[6] Y. Kuramoto, Effects of diffusion on the fluctuations in open chemical systems, Progr. Theor. Phys. 52 (1974) 711–713.
[7] C. Van Den Broeck, W. Horsthemke, M. Malek-Mansour, On the diffusion operator of the multivariate master equation, Physica A 89 (2) (1977) 339–352.
[8] M.A. Burschka, Fluctuations in diffusion reaction systems. I: adiabatic elimination of transport modes from a mesoscopic *n*-body system and the omega-expansion, J. Stat. Phys. 45 (3–4) (1986) 715–744.
[9] F. Baras, M.M. Mansour, Reaction–diffusion master equation: a comparison with microscopic simulations, Phys. Rev. E 54 (6) (1996) 6139–6148.
[10] D. Bernstein, Simulating mesoscopic reaction–diffusion systems using the Gillespie algorithm, Phys. Rev. E 71 (4) (2005) 041103.
[11] B. Bayati, P. Chatelain, P. Koumoutsakos, Multiresolution stochastic simulations of reaction–diffusion processes, Phys. Chem. Chem. Phys. 10 (39) (2008) 5963–5966.
[12] D. Rossinelli, B. Bayati, P. Koumoutsakos, Accelerated stochastic and hybrid methods for spatial simulations of reaction–diffusion systems, Chem. Phys. Lett. 451 (1-3) (2008) 136–140.
[13] S. Engblom, L. Ferm, A. Hellander, P. Lotstedt, Simulation of stochastic reaction–diffusion processes on unstructured meshes, SIAM J. Sci. Comput. 31 (3) (2009) 1774–1797.
[14] S. Lampoudi, D.T. Gillespie, L.R. Petzold, The multinomial simulation algorithm for discrete stochastic simulation of reaction–diffusion systems, J. Chem. Phys. 130 (9) (2009) 094104.
[15] N.G. Van Kampen, Stochastic Processes in Physics and Chemistry, second ed., North Holland, 2001.
[16] A.B. Bortz, M.H. Kalos, J.L. Lebowitz, A new algorithm for Monte Carlo simulation of Ising spin systems, J. Comput. Phys. 17 (1) (1975) 10–18.
[17] D.T. Gillespie, A general method for numerically simulating the stochastic time evolution of coupled chemical reactions, J. Comput. Phys. 22 (4) (1976) 403–434.
[18] D.T. Gillespie, Stochastic simulation of chemical kinetics, Annu. Rev. Phys. Chem. 58 (2007) 35–55.
[19] D.T. Gillespie, A rigorous derivation of the chemical master equation, Physica A: Stat. Theor. Phys. 188 (1–3) (1992) 404–425.
[20] Randall J. Leveque, Finite Volume Methods for Hyperbolic Problems, Cambridge University Press, 2002.
[21] L. Ferm, A. Hellander, P. Lotstedt, An adaptive algorithm for simulation of stochastic reaction–diffusion processes, J. Comput. Phys. 229 (2) (2010) 343–360.
[22] B. Drawert, M.J. Lawson, L. Petzold, M. Khammash, The diffusive finite state projection algorithm for efficient simulation of the stochastic reaction–diffusion master equation, J. Chem. Phys. 132 (7) (2010) 074101.
[23] B. Munsky, M. Khammash, The finite state projection algorithm for the solution of the chemical master equation, J. Chem. Phys. 124 (4) (2006) 044101.
[24] D.F. Martin, P. Colella, D. Graves, A cell-centered adaptive projection method for the incompressible Navier–Stokes equations in three dimensions, J. Comput. Phys. 227 (3) (2008) 1863–1886.

[25] R.A. Fisher, The wave of advance of advantageous genes, Ann. Eugenics 7 (1937) 355–369.
[26] J.E. Pearson, Complex patterns in a simple system, Science 261 (5118) (1993) 189–192.
[27] S.A. Isaacson, The reaction–diffusion master equation as an asymptotic approximation of diffusion to a small target, SIAM J. Appl. Math. 70 (1) (2009) 77–111.
[28] E. Mjolsness, D. Orendorff, P. Chatelain, P. Koumoutsakos, An exact accelerated stochastic simulation algorithm, J. Chem. Phys. 130 (14) (2009) 144110.
[29] D.T. Gillespie, Deterministic limit of stochastic chemical kinetics, J. Phys. Chem. B 113 (6) (2009) 1640–1644.
[30] I.D. Mishev, Finite volume methods on Voronoi meshes, Numer. Meth. Partial Differ. Eqn. 14 (2) (1998) 193–212.
[31] Z.Q. Cai, J. Douglas, M. Park, Development and analysis of higher order finite volume methods over rectangles for elliptic equations, Adv. Comput. Math. 19 (1–3) (2003) 3–33.
[32] R. Erban, S.J. Chapman, Stochastic modelling of reaction–diffusion processes: algorithms for bimolecular reactions, Phys. Bio. 6 (4) (2009) 046001.
[33] B. Cockburn, P.A. Gremaud, A priori error estimates for numerical methods for scalar conservation laws, Math. Comput. 66 (218) (1997) 547–572.
[34] J.D. Murray, Mathematical Biology: An Introduction, Springer-Verlag, 2002.
[35] D.T. Gillespie, Approximate accelerated stochastic simulation of chemically reacting systems, J. Chem. Phys. 115 (4) (2001) 1716–1733.
[36] D.L. Brown, G.S. Chesshire, W.D. Henshaw, D.J. Quinlan. Overture: an object-oriented software system for solving partial differential equations in serial and parallel environments. in: Proceedings Eighth SIAM Conference on Parallel Processing for Scientific Computing, 1997, 8 pp.
[37] W.D. Henshaw, D.W. Schwendeman, Parallel computation of three-dimensional flows using overlapping grids with adaptive mesh refinement, J. Comput. Phys. 227 (16) (2008) 7469–7502.